Experimental details

Synthesis. The powders were synthesized via a wet chemical route, as described in ref. [1]. Two compositions with nominal La/W atomic ratio 5.3 (LWO53) and 5.7 (LWO57) were fabricated. Final sintering temperature was 1500 °C.

Modeling tools. Initial calculations were performed with atomistic techniques using interatomic potentials and effective energy minimization (within the GULP code) [2]. Parameters for the shell model for La and potentials for La-O and O-O are described in Ref. [3], and parameters for the shell model for W and O, and potential for W-O are described in Ref. [4]. DFT-based calculations were performed using the generalized gradient approximation functional by Perdew, Burke and Ernzerhof (GGA-PBE) [5] and periodic boundary conditions as implemented in VASP [6]. The cell shape was fixed to cubic and the non-fixed atomic positions were optimized until the residual forces for the relaxed atoms were within 0.02 eVÅ^{-1}.

Crystallographic characterization. Patterns from ultra-high resolution synchrotron X-Ray diffraction (SPD; ID31 diffractometer, ESRF, Grenoble) and neutron powder diffraction (NPD; D2B diffractometer; of ILL in its high resolution mode) were collected at room temperature. Selected area electron diffraction (SAED) and high resolution transmission electron microscopy (HRTEM) studies were carried out for both compositional end members in a Jeol 2100 TEM operating at 200kV.

X-ray Photoelectron Spectroscopy characterization. XPS was performed in a Kratos Axis Ultra^{DLD} spectrometer.

Electrical characterization. Pt electrodes (Ferro 6512-0410 Pt ink) were painted on each side of the sintered specimens and fired at 1000 ºC for 1 hour. The electrical characterization was performed in ProboStat measurement cells (NorECs AS, Norway). Impedance spectra were obtained using a frequency response analyzer (Novocontrol Alpha A, Novocontrol Technologies) in the frequency range 0.1 Hz - 1 MHz at an AC voltage of 100 mV RMS. The total a.c. conductivity was measured as a function of pO_2 at 1100°C. This is only included in as a supplementary material to show the donor doping effect of tungsten in this material.

[1] A. Magrasó, C. Frontera, D. Marrero-López, P. Núñez, *Dalton Trans.*, 2009, 10273–10283

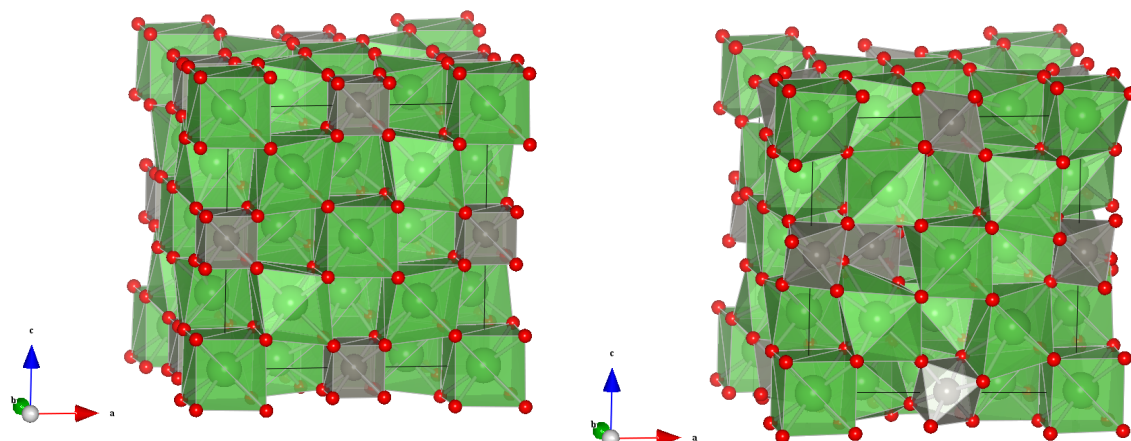[2] J.D. Gale, *J. Chem. Soc.– Far. Trans.* 1997, **93,** 629-637

[3] M.S. Kahn, M.S. Islam, D.R. Bates, *J. Phys. Chem. B*, 1998, 102, 30991

[4] M.S. Islam, S. Lazure, R.-N. Vannier, G. Nowogrocki and G. Mairesse, *J. Mater. Chem.*, 1998, 3, 655-660

[5] J. P. Perdew, K. Burke and M. Ernzerhof, *Phys. Rev. Lett.*, 1996, 77, 3865-3868.

[6] G. Kresse and J. Furthmuller, *Phys. Rev. B*, 1996, 54, 11169-11186

DFT and potentials-based calculations

Figure SI-4. (left) "Old" schematic representation of the crystal structure from ref. [1] showing the 8-fold WO_8 cubes. This configuration, however, results in unphysical structures. The formula corresponds to $La_{28}W_4O_{54}v_{10}$ (the structure has 64 oxygen positions, from which 54 are occupied, and 10 are vacant). The "interstitial" tungsten reported in [1] was disregarded due to the low occupancy level and the low confidence related to locating this remaining tungsten. (right) Final structure for $La_{27}W_5O_{55.5}v_{0.5}$ ($La_{28-x}W_{4+x}O_{54+\delta}v_{2-\delta}$ when x=1: the structure has 56 oxygen positions, from which 54 are occupied, and 2 are vacant, and the vacant oxygen sites are filled up as a function of tungsten content). The La8(La7) polyhedra are drawn to show the similarities between the two structural models. Note that the WO_6 octahedra can tilt in various directions, showing disorder.
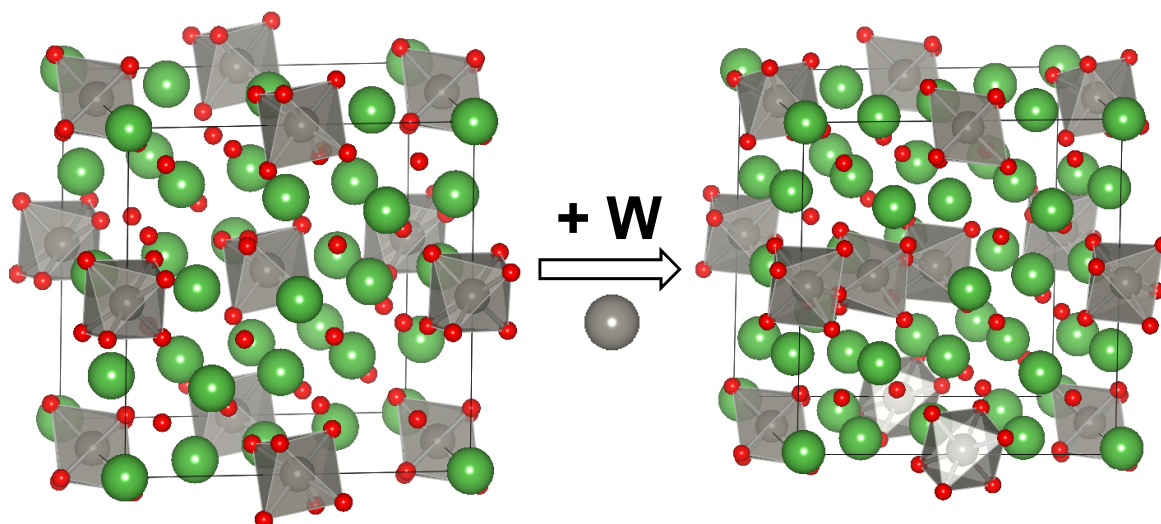
Figure SI-5. (left) The mother structure $La_{28}W_4O_{54}v_2$ (not stable, it is not possible to synthesize) can dissolve W in the La2 site (right) and form more stable structures. Note the reduction in amount of "oxygen vacancies" from $La_{28}W_4O_{54}v_2$ to $La_{27}W_5O_{55.5}v_{0.5}$ in the case that <u>one</u> W replaces La2.

Conductivity and correlation to point defect chemistry
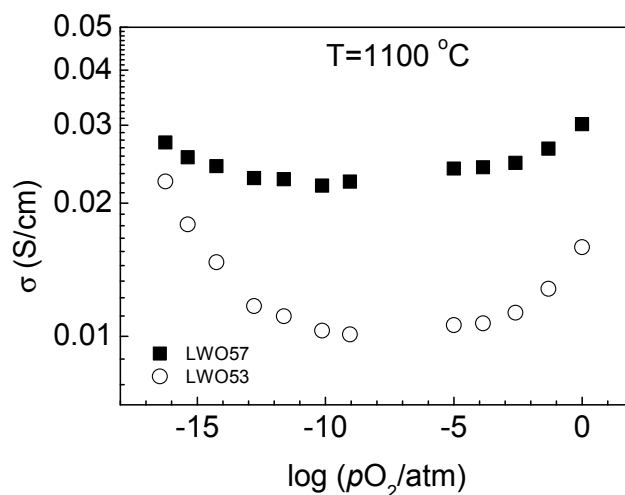
Figure SI-6. Dependency of the total electrical conductivity on oxygen partial pressure at 1100 °C in wet atmospheres.

The flat regime at intermediate oxygen partial pressures represents ionic conductivity, while the contributions at either side represent n- and p-type electronic conductivities, in accordance with previous studies [7].

The ionic conductivity is lower for LWO53 compared to LWO57, while the relative contribution of n-type conductivity at low pO_2 in LWO53 is higher than in LWO57. The electrons remain minor defects concentration-wise, but their higher mobility ensures they have a tangible effect on the total conductivity. This is in accordance with the model $La_{28-x}W_{4+x}O_{54+\delta}v_{2-\delta}$: The W on La site ($W_{La2}$) acts as a donor, which is mainly compensated by oxide ions, filling the oxygen vacancies. Therefore, more W inhibits ionic conductivity due to a lower concentration of oxygen vacancies. This is dealt in more detail in a recent publication by Erdal *et al.* [8] .

[7] R. Haugsrud, *Solid State Ionics* 2007, **178**, 555-560
[8] S. Erdal, L.-E. Kalland, R. Hancke, J. Polfus, R. Haugsrud, T. Norby, A. Magrasó, *Int. J. Hydrogen Energy*, 2011, *in press*, DOI: 10.1016/j.ijhydene.2011.11.093.